DTC based on five-level SVM with balancing strategy of sensorless DSSM

Elakhdar Benyoussef[1], Said Barkat[2]

[1]Department of Electrical Engineering, University of Kasdi Merbah, Ouargla 30000, BP. 511 Algeria,

[2]Faculty of Technology, Department of Electrical Engineering, University of M'sila, Ichbilia Street, M'sila 28000, BP 166, Algeria.

Corresponding author: lakhdarbenyoussef@yahoo.com

Received: September 2, 2022. Revised: February 1, 2023. Accepted: February 24, 2023. Published: March 13, 2023.

Abstract— This paper presents a direct torque control based on multilevel space vector modulation of a double star synchronous machine operating without speed sensor. Each star of the machine is supplied by a five-level diode-clamped inverter. This topology of multilevel inverters represents one of the most interesting solutions to increase voltage and power levels and to achieve high quality voltage waveforms. However, a very important issue in using diode-clamped inverters is the ability to guarantee the stability of the DC-link capacitor voltages. To overcome this problem the multilevel space vector modulation equipped by a balancing strategy is proposed to suppress the unbalance of DC-link capacitor voltages. For achieving high performances control of the multiphase drive, the proposed control method needs accurate information about rotor position and rotor speed. To this end, they are estimated by using Luenberger observer.

Keywords— Double star synchronous machine, multilevel diode clamped inverter, balancing strategy, space vector modulation, direct torque control.

I. Introduction

The concept of power segmentation has been emerged to allow the use of voltage source inverter with reduced size power electronic devices. There are different ways to achieve this requirement. One of them is to use multilevel inverter fed AC machines; this solution has been greatly developed and studied in the past. Another way is to use multiphase machines or multi-star machines. For this kind of structure, each phase or each star is fed by its own inverter. The major advantages of using a multiphase machine instead of a three-phase machine are detailed in [1, 2]. Other potential advantages concern the reliability of the drive system, unlike in normal three-phase machine; the loss of one phase in a multiphase machine drive system does not prevent the machine from starting and running.

Research interest in the area of multiphase machines has been steadily increasing during the past decade. High power drives employing multiphase machines are required in a lot of applications, such as traction, electric marine propulsion and electric aircraft [3, 4].

In multiphase machine drive systems, more than three-phase windings are implemented in the same stator. Among the multiphase machines, five-phase and six-phase induction or synchronous machines are the most considered in the literature [1]. One common example of such structure is the double star synchronous machine (DSSM). This machine has two sets of three-phase windings spatially phase shifted by 30 electrical degrees and each set is fed generally by a two-level inverter [2]. In order to accomplish both objectives: power segmentation, and ensure a high reliability, the use of multiphase machines supplied by multilevel inverters has been recognized as a viable approach to obtain high power ratings without increasing the stator current per phase.

Multilevel inverters can frequently be seen in high-power high-voltage applications due to their numerous merits. The outstanding advantage of multilevel inverters is their smaller output voltage step, which results in high power quality, lower harmonic components, better electromagnetic compatibility, and lower switching losses [5]. Among all the multilevel topologies, the most commonly used multilevel topology is the diode-clamped inverter (DCI). However, the main drawback of this type of inverter is the problem of voltage imbalance in DC capacitors [6]. For this reason several methods are proposed in the literature to suppress the unbalance of DC link capacitor voltages [7]. Among these methods the multilevel space vector modulation (SVM) has emerged as the most promising solution to guarantee the stability of DC-side voltages [6].

In the other hand, the multilevel direct torque control (DTC) of electrical drives has become an attracting topic in research and academic community over the past decade. Like an every control method has some advantages and disadvantages, DTC method has too. Some of its advantages are: a suitable control method for inverter-fed AC drives, characterized by a fast dynamic response, structural simplicity, and low sensitivity to parameter variations. Also, there are several disadvantages like high current, flux and torque ripple, torque control difficulties at very low speed, and especially variable switching frequency behavior [2]. In order to overcome these problems, the direct torque control based on space vector modulation (DTC-SVM) was proposed in [8]. DTC-SVM technique has also a simple structure and provides dynamic behavior comparable with classical DTC with constant switching frequency.

In order to ensure the balance of the DC-link capacitors voltages and to improve the performances of the multiphase drive, the five-level DTC-SVM with balancing strategy is proposed in this paper.

In the aim to produce better control performance, researchers are interested by sensorless speed control. The elimination of the speed sensor reduces the hardware complexity, size and cost, and increases the reliability of the drive system. A lot of attention has been paid recently to the development of sensorless control algorithms for electrical drives [8, 9]. Several speed sensorless control schemes have been suggested in literature in order to eliminate the speed sensor: Model reference adaptive system [10], sliding mode observer and Kalman filtering technique [11] may be are the prospective state observation methodologies for the electric machines. In this work a simple approach based on Luenberger observer is adopted. This observer is known by its futures such as order reduction control, and simple hard implementation.

The present paper is organized as follows. In Section II, the DSSM model is reported. Section III details the SVM algorithm for five-level DCI. In Section IV, the DTC approach based on SVM in *x-y* reference frame is investigated. Speed estimation using Luenberger observer is proposed in section V. Comparative study between two-level conventional DTC and two-level DTC-SVM for sensorless DSSM is presented in the section VI. The two-level DTC-SVM is compared with five-level DTC-SVM in the section VII. A balancing strategy for DC voltages is developed in section VIII. In the section IX, the simulation results related to the five-level DTC-SVM with balancing strategy are presented and discussed.

II. Double Star Synchronous Machine Model

The modeling of the machine is based on the usual assumptions such as the effect of saturation is neglected, the distribution of induction along the air-gap is sinusoidal, and the effect of the dampers is neglected. A schematic of the stator and rotor windings for a double star synchronous machine is given in Fig. 1.

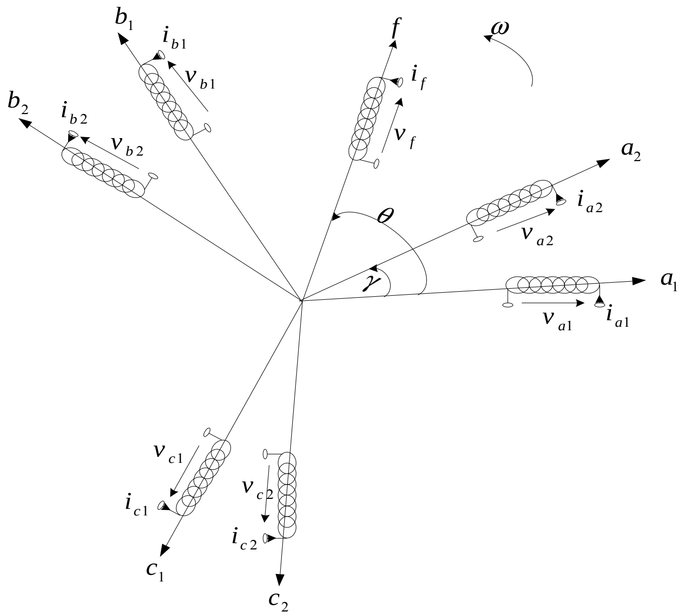

Fig. 1 double star synchronous machine stator winding scheme.

For an idealized DSSM the following equations of the instantaneous stator phase voltages can be written:

$$\begin{cases} v_{s1} = R_s i_{s1} + \dfrac{d\phi_{s1}}{dt} \\ v_{s2} = R_s i_{s2} + \dfrac{d\phi_{s2}}{dt} \end{cases} \tag{1}$$

With: $v_{s1} = [v_{a1} \quad v_{b1} \quad v_{c1}]$, $v_{s2} = [v_{a2} \quad v_{b2} \quad v_{c2}]$

The rotor voltage equation is given by:

$$v_f = R_f i_f + \frac{d}{dt}\phi_f \tag{2}$$

The original six dimensional system of the machine can be decomposed into three orthogonal subspaces (α,β), (z_1, z_2) and (z_3, z_4), using the following transformation.

$$[T] = \frac{1}{\sqrt{3}} \begin{pmatrix} 1 & -\frac{1}{2} & -\frac{1}{2} & \frac{\sqrt{3}}{2} & -\frac{\sqrt{3}}{2} & 0 \\ 0 & \frac{\sqrt{3}}{2} & -\frac{\sqrt{3}}{2} & \frac{1}{2} & \frac{1}{2} & -1 \\ 1 & -\frac{1}{2} & -\frac{1}{2} & -\frac{\sqrt{3}}{2} & \frac{\sqrt{3}}{2} & 0 \\ 0 & -\frac{\sqrt{3}}{2} & \frac{\sqrt{3}}{2} & \frac{1}{2} & \frac{1}{2} & -1 \\ 1 & 1 & 1 & 0 & 0 & 0 \\ 0 & 0 & 0 & 1 & 1 & 1 \end{pmatrix} \tag{3}$$

II.1. Stator fixed system (α,β)

The dynamic model describing the machine in α-β reference can be given by:

$$\begin{pmatrix} v_\alpha \\ v_\beta \end{pmatrix} = R_s \begin{pmatrix} i_\alpha \\ i_\beta \end{pmatrix} + \begin{pmatrix} l_{fs}+3M_{ss} & 0 \\ 0 & l_{fs}+3M_{ss} \end{pmatrix} \frac{d}{dt}\begin{pmatrix} i_\alpha \\ i_\beta \end{pmatrix} + \sqrt{3}M_{sf}\frac{d}{dt}\begin{pmatrix} \cos(\theta) \\ \sin(\theta) \end{pmatrix} i_f + M_{sfm}\begin{pmatrix} 3\cos(2\theta) & 3\sin(2\theta) \\ 3\sin(2\theta) & -3\cos(2\theta) \end{pmatrix}\frac{d}{dt}\begin{pmatrix} i_\alpha \\ i_\beta \end{pmatrix} \tag{4}$$

II.2. Stator flux fixed system (x,y)

In order to control directly and independently the flux and the torque the model of the DSSM is expressed in the stator flux reference frame by applying the following rotation transformation.

$$\begin{pmatrix} F_x \\ F_y \end{pmatrix} = \begin{pmatrix} \cos(\theta_s) & \sin(\theta_s) \\ -\sin(\theta_s) & \cos(\theta_s) \end{pmatrix}\begin{pmatrix} F_\alpha \\ F_\beta \end{pmatrix} \tag{5}$$

The electrical equations become:

$$\begin{cases} v_x = R_s i_x + \dfrac{d\phi_x}{dt} - \omega_s\phi_y \\ v_y = R_s i_y + \dfrac{d\phi_y}{dt} + \omega_s\phi_x \end{cases} \tag{6}$$

The stator flux linkage equations in *x-y* reference frame are as follows:

$$\begin{cases} \phi_x = L_d i_x + \phi_f \cos(\delta) \\ \phi_y = L_q i_y - \phi_f \sin(\delta) \end{cases} \tag{7}$$

The electromagnetic torque of DSSM is expressed as:

$$T_{em} = p\left(\phi_x i_y - \phi_y i_x\right) \tag{8}$$

II.3. Rotor flux fixed system (d,q)

To express the stator equations in the rotor reference frame, the following rotation transformation is appropriate:

$$P(\theta) = \begin{pmatrix} \cos(\theta) & \sin(\theta) \\ -\sin(\theta) & \cos(\theta) \end{pmatrix} \tag{9}$$

With this transformation, the voltage vector components in α-β plane can be expressed in the *d-q*plane as:

$$\begin{cases} v_d = R_s i_d + \dfrac{d\phi_d}{dt} - \omega\phi_q \\ v_q = R_s i_q + \dfrac{d\phi_q}{dt} + \omega\phi_d \end{cases} \tag{10}$$

With

$\phi_d = L_d i_d + M_{fd} i_f$, $\phi_q = L_q i_q$, $L_d = l_{sf} + 3M_{ss} + 3M_{sfm}$

$L_q = l_{sf} + 3M_{ss} - 3M_{sfm}$, $M_{fd} = \sqrt{3}M_{sf}$

The mechanical equation is given by:

$$J\frac{d\Omega}{dt} = T_{em} - T_L - f_r\Omega \tag{11}$$

The electromagnetic torque generated by the machine is:

$$T_{em} = p\left(\phi_d i_q - \phi_q i_d\right) \tag{12}$$

III. Five-Level Space Vector Modulation

In Fig. 2 one phase-leg of a five-level DCI is displayed. With this configuration five levels of voltage can be generated between points "*a*" and the neutral point *o*. Depending on which switches that are switched v_{c3}, $v_{c3}+v_{c4}$, 0, $-v_{c2}$ and $-(v_{c1}+v_{c2})$ can be achieved.

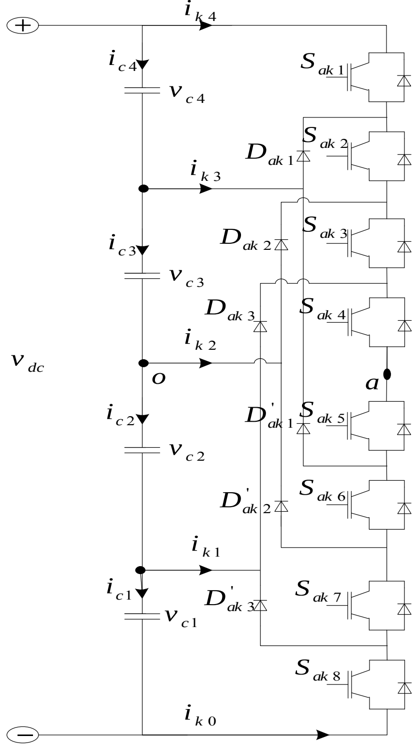

Fig. 2 one phase-leg for a five-level DCI Inverter (*k*=1 for first inverter and *k*=2 for second inverter).

In table 1 the different states and corresponding output voltage v_{xko} of the five-level DCI are shown. Note that there is the possibility to only turn ON (and OFF) every switch once per cycle, meaning that the inverter can generate a stepped sinusoidal waveform with a fundamental switching frequency.

State	S_{xk1}	S_{xk2}	S_{xk3}	S_{xk4}	S_{xk5}	S_{xk6}	S_{xk7}	S_{xk8}	v_{xko}
4	1	1	1	1	0	0	0	0	$v_{c3}+v_{c4}$
3	0	1	1	1	1	0	0	0	v_{c3}
2	0	0	1	1	1	1	0	0	0
1	0	0	0	1	1	1	1	0	$-v_{c2}$
0	0	0	0	0	1	1	1	1	$-(v_{c1}+v_{c2})$

Table 1 switching state of five-level DCI.

The Boolean function F_{xki} associated to the switch S_{xki} is defined by:

$$F_{xki} = \begin{cases} 1 & S_{xki} \;\; is \;\; ON \\ 0 & S_{xki} \;\; is \;\; OFF \end{cases} \tag{13}$$

With: ($i= 1…8, k=1, 2, x=a, b$ or c).

For each leg of the inverter, five connections functions can be defined:

$$\begin{cases} F_{cxk1} = F_{xk1}F_{xk2}F_{xk3}F_{xk4} \\ F_{cxk2} = F_{xk2}F_{xk3}F_{xk4}F_{xk5} \\ F_{cxk3} = F_{xk3}F_{xk4}F_{xk5}F_{xk6} \\ F_{cxk4} = F_{xk4}F_{xk5}F_{xk6}F_{xk7} \\ F_{cxk5} = F_{xk5}F_{xk6}F_{xk7}F_{xk8} \end{cases} \tag{14}$$

Finally, the phase voltages v_{ak}, v_{bk}, v_{ck} can be written as:

$$\begin{pmatrix} v_{ak} \\ v_{bk} \\ v_{ck} \end{pmatrix} = \begin{pmatrix} F_{cak1} & F_{cak2} & F_{cak3} & F_{cak4} & F_{cak5} \\ F_{cbk1} & F_{cbk2} & F_{cbk3} & F_{cbk4} & F_{cbk5} \\ F_{cck1} & F_{cck2} & F_{cck3} & F_{cck4} & F_{cck5} \end{pmatrix} \begin{pmatrix} v_{c3}+v_{c4} \\ v_{c3} \\ 0 \\ -v_{c2} \\ -(v_{c1}+v_{c2}) \end{pmatrix} \tag{15}$$

Fig. 3 depicts the switching states distribution in the complex plane for the five-level DCI. For this inverter *125* different combinations of the switching function are possible, but most of them correspond to the same voltage space vector. In particular, as the most external vectors are realizable with only one combination of the switching functions, the inner vectors are realizable in different redundant ways.

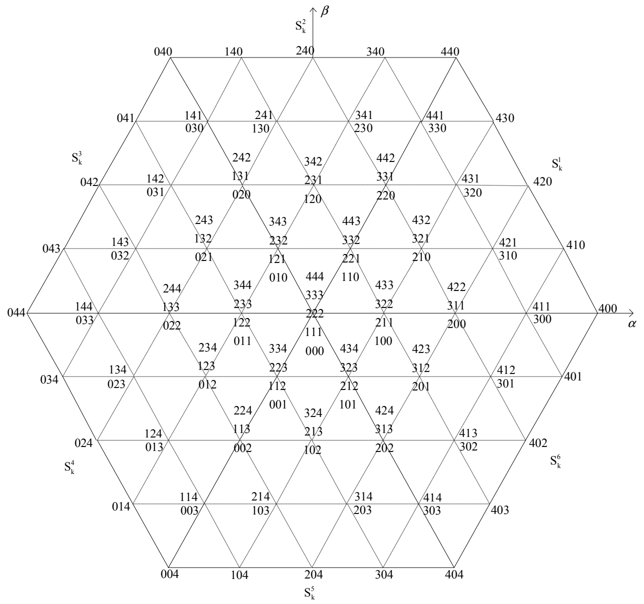

Fig. 3 possible switching states of a five-level DCI.

The SVM methods provide flexibility to select and optimize switching patterns to (i) minimize harmonics, (ii) modify the switching pattern to carry out DC-capacitor voltages balancing task with no requirement for additional power circuitry, and (iii) minimize switching frequency for high power applications. However, real-time implementation of the conventional SVM strategies is faced with time limits due to the calculation overhead time. Therefore, fast algorithms are required to overcome complexity of calculations. A fast SVM algorithm can save the processor execution time to perform the required calculations of DC-capacitor voltages balancing task.

III.1. Determination of the sector numbers

The reference vector magnitude and its angle are determined from:

$$\begin{cases} U_{refk} = \sqrt{u_{ref\alpha k}^2 + u_{ref\beta k}^2} \\ \vartheta_k = \tan2^{-1}\left(\dfrac{u_{ref\beta k}}{u_{ref\alpha k}}\right) \end{cases} \tag{16}$$

Where the $\tan 2^{-1}$ function returns an angle $-\pi \le \vartheta_k \le \pi$ which is converted into the range $0 \le \vartheta_k \le 2\pi$ by a C subroutine.

The sector numbers are given by:

$$S_k^i = ceil\left(\frac{\vartheta_k}{\pi/3}\right) \in \left\{S_k^1,\, S_k^2,\, S_k^3,\, S_k^4,\, S_k^5,\, S_k^6\right\} \tag{17}$$

Where *ceil* is the C-function that adjusts any real number to the nearest, but higher, integer [e.g. *ceil* (*3.1*) =*4*].

III.2. Identification of the triangles

The reference vector is projected on the two axes making 60^o between them. In each sector S_k^i, the components $u_{refk1}^{S_k^i}$ and $u_{refk2}^{S_k^i}$ are given by:

$$\begin{aligned} u_{refk1}^{S_k^i} &= 4M_k\left(\cos(\vartheta_k - (S_k^i - 1)\frac{\pi}{3}) - \frac{1}{\sqrt{3}}\sin(\vartheta_k - (S_k^i - 1)\frac{\pi}{3})\right) \\ u_{refk2}^{S_k^i} &= 4M_k\left(\frac{2}{\sqrt{3}}\sin(\vartheta_k - (S_k^i - 1)\frac{\pi}{3})\right) \end{aligned} \tag{18}$$

The modulation factor M_k is given by:

$$M_k = \frac{U_{refk}}{v_{dc}\sqrt{2/3}} \tag{19}$$

In order to determine $\Delta_q^{S_k^i}$ the number of the triangle in a sector S_k^i, the two following entireties are to be defined:

$$\begin{aligned} l_{k1}^{S_k^i} &= \mathrm{int}(u_{refk1}^{S_k^i}) \\ l_{k2}^{S_k^i} &= \mathrm{int}(u_{refk2}^{S_k^i}) \end{aligned} \tag{20}$$

Where : *int* is a function which gives the whole part of a given real number.

The Fig. 4 presents the projection of U_{refk} in the first sector [16].

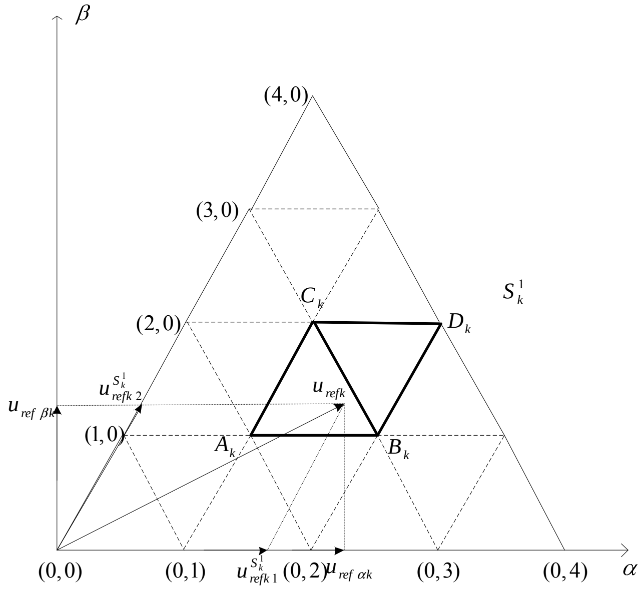

Fig. 4 space voltage vectors of a five-level DCI in the first sector.

For a specified voltage reference formed by two vectors $u_{refk1}^{S_k^i}$ and $u_{refk2}^{S_k^i}$, the coordinates of the tops A_k, B_k, C_k and D_k are given by:

$$\begin{cases} \left(u_{A_{k1}}^{\Delta_q^{S_k^i}},\ u_{A_{k2}}^{\Delta_q^{S_k^i}}\right) = \left(l_{k1}^{S_k^i},\ l_{k2}^{S_k^i}\right) \\ \left(u_{B_{k1}}^{\Delta_q^{S_k^i}},\ u_{B_{k2}}^{\Delta_q^{S_k^i}}\right) = \left(l_{k1}^{S_k^i}+1,\ l_{k2}^{S_k^i}\right) \\ \left(u_{C_{k1}}^{\Delta_q^{S_k^i}},\ u_{C_{k2}}^{\Delta_q^{S_k^i}}\right) = \left(l_{k1}^{S_k^i},\ l_{k2}^{S_k^i}+1\right) \\ \left(u_{D_{k1}}^{\Delta_q^{S_k^i}},\ u_{D_{k2}}^{\Delta_q^{S_k^i}}\right) = \left(l_{k1}^{S_k^i}+1,\ l_{k2}^{S_k^i}+1\right) \end{cases} \tag{21}$$

The following criteria (22) and (23) determine if the reference vector is located in the triangle formed by the tops A_k, B_k and C_k or in that formed by the tops B_k, C_k and D_k.

u_{refk} is in the triangle $A_kB_kC_k$ if:

$$u_{refk1}^{S_k^i} + u_{refk2}^{S_k^i} < l_{k1}^{S_k^i} + l_{k2}^{S_k^i} + 1 \tag{22}$$

u_{refk} is in the triangle $B_kC_kD_k$ if:

$$u_{refk1}^{S_k^i} + u_{refk2}^{S_k^i} \geq l_{k1}^{S_k^i} + l_{k2}^{S_k^i} + 1 \tag{23}$$

III.3. Calculation of application times

The application times are calculated by:

$$\begin{cases} t_{B_k}^{\Delta_q^{S_k^i}} = \left(u_{refk1}^{S_k^i} - l_{k1}^{S_k^i}\right)T_s \\ t_{C_k}^{\Delta_q^{S_k^i}} = \left(u_{refk2}^{S_k^i} - l_{k2}^{S_k^i}\right)T_s \\ t_{A_k}^{\Delta_q^{S_k^i}} = T_s - \left(t_{B_k}^{\Delta_q^{S_k^i}} + t_{C_k}^{\Delta_q^{S_k^i}}\right) \end{cases} \tag{24}$$

Where:

$t_{A_k}^{\Delta_q^{S_k^i}}, t_{B_k}^{\Delta_q^{S_k^i}}, t_{C_k}^{\Delta_q^{S_k^i}}$:are times of application of the vectors $u_{A_k}^{\Delta_q^{S_k^i}}, u_{B_k}^{\Delta_q^{S_k^i}}, u_{C_k}^{\Delta_q^{S_k^i}}$ respectively.

With $q=1,\dots,16$, and $S_k^i = S_k^1,\dots,S_k^6$.

III.4. Effects of different switching states on DC intermediate branch currents

To develop a mathematical model that describes the average current in the DC-intermediate branches, the contributions of different switching states to the DC-intermediate branch currents and the relationship between the DC-intermediate branch currents and the AC- side currents for each switching state are required. The proposed SVM algorithm intrinsically maps all sectors to the first sector S_k^1, only sector S_k^1 is considered and then based on minor adjustments; the analysis is generalized for all sectors. Effects of switching states on DC-intermediate branch currents, i.e. i_{k3}, i_{k2} and i_{k1}, and their relationship with AC side currents, i.e. i_{ak}, i_{bk}, and i_{ck}, in sector S_k^1 are shown in table 2.

Switching state	i_{k3}	i_{k2}	i_{k1}	Switching state	i_{k3}	i_{k2}	i_{k1}
400	0	0	0	200	0	i_{ak}	0
410	0	0	i_{bk}	432	i_{bk}	i_{ck}	0
420	0	i_{bk}	0	321	i_{ak}	i_{bk}	i_{ck}
430	i_{bk}	0	0	210	0	i_{ak}	i_{bk}
440	0	0	0	442	0	i_{ck}	0
411	0	0	$-i_{ak}$	331	$-i_{ck}$	0	i_{ck}
300	i_{ak}	0	0	220	0	$-i_{ck}$	0
421	0	i_{bk}	i_{ck}	433	$-i_{ak}$	0	0
310	i_{ak}	0	i_{bk}	322	i_{ak}	$-i_{ak}$	0
431	i_{bk}	0	i_{ck}	211	0	i_{ak}	$-i_{ak}$
320	i_{ak}	i_{bk}	0	100	0	0	i_{ak}
441	0	0	i_{ck}	443	i_{ck}	0	0
330	$-i_{ck}$	0	0	332	$-i_{ck}$	i_{ck}	0
422	0	$-i_{ak}$	0	221	0	$-i_{ak}$	i_{ck}
311	i_{ak}	0	$-i_{ak}$	110	0	0	$-i_{ak}$

Table 2 relations between DC-side currents and phase currents for different switching states in the first sector S_k^1.

In order to find similar relations between currents, as shown in Table 2, Table 3 gathers the various exchanges needed to be carried out between the phase currents in the first sector and phase currents in the other sectors.

S_k^1	S_k^2	S_k^3	S_k^4	S_k^5	S_k^6
i_{ak}	$i_{ak} \to i_{bk}$	$i_{ak} \to i_{bk}$	$i_{ak} \to i_{ck}$	$i_{ak} \to i_{ck}$	i_{ak}
i_{bk}	$i_{bk} \to i_{ak}$	$i_{bk} \to i_{ck}$	i_{bk}	$i_{bk} \to i_{ak}$	$i_{bk} \to i_{ck}$
i_{ck}	i_{ck}	$i_{ck} \to i_{ak}$	$i_{ck} \to i_{ak}$	$i_{ck} \to i_{bk}$	$i_{ck} \to i_{bk}$

Table 3. Interchanging phase currents between S_k^1 and S_k^i, $i = 2,...,6$.

IV. DIRECT TORQUE CONTROL BASED ON SPACE VECTOR MODULATION

In DTC control scheme the reference stator flux magnitude and reference electromagnetic torque are compared with their estimated values. The flux and torque errors are delivered to *PI* controllers, which generate the reference stator voltage components in stator flux coordinates (v_x^*, v_y^*) . These voltages are transformed to stationary coordinates using the estimated stator flux position angle $\hat{\theta}_s$. The reference stator voltage components $(v_{\alpha k}^*, v_{\beta k}^*)$ are delivered to space vector modulator, which generates the switching signals necessary to control power transistors of the inverter [12]. So, the next step is to transform x-y variables in the stator reference frame using the following transformations.

$$\begin{pmatrix} v_{\alpha 1}^* \\ v_{\beta 1}^* \\ v_{\alpha 2}^* \\ v_{\beta 2}^* \end{pmatrix} = \begin{pmatrix} \cos(\theta_s) & \sin(\theta_s) \\ -\sin(\theta_s) & \cos(\theta_s) \\ \cos(\theta_s - \gamma) & \sin(\theta_s - \gamma) \\ -\sin(\theta_s - \gamma) & \cos(\theta_s - \gamma) \end{pmatrix} \begin{pmatrix} v_x^* \\ v_y^* \end{pmatrix} \tag{25}$$

The stator voltage estimator is based on the following equation:

$$\begin{pmatrix} \hat{v}_\alpha \\ \hat{v}_\beta \end{pmatrix} = [T] \begin{pmatrix} \hat{v}_{s1} \\ \hat{v}_{s2} \end{pmatrix} \tag{26}$$

With: $\hat{v}_{s1} = [\hat{v}_{a1} \quad \hat{v}_{b1} \quad \hat{v}_{c1}]$ and $\hat{v}_{s2} = [\hat{v}_{a2} \quad \hat{v}_{b2} \quad \hat{v}_{c2}]$
$\hat{v}_{xk}$ are computed using (15).

The stator flux is estimated from the measure of stator currents and the estimation of stator voltages and their transformation in the α-β subspace. So:

$$\begin{cases} \hat{\phi}_\alpha = \int_0^t (\hat{v}_\alpha - R_s i_\alpha) d\tau + \hat{\phi}_\alpha(0) \\ \hat{\phi}_\beta = \int_0^t (\hat{v}_\beta - R_s i_\beta) d\tau + \hat{\phi}_\beta(0) \end{cases} \tag{27}$$

The stator flux magnitudeis given by:

$$\hat{\phi}_s = \sqrt{\hat{\phi}_\alpha^2 + \hat{\phi}_\beta^2} \tag{28}$$

The stator flux angle is calculated by:

$$\hat{\theta}_s = \tan 2^{-1}\left(\frac{\hat{\phi}_\beta}{\hat{\phi}_\alpha}\right) \tag{29}$$

The complete set of DSSM model equations can be written in stator flux coordinate system x-y. This system of coordinates rotates with the stator flux angular speed Ω_s. This angular speed is defined as follows: $\Omega_s = d\theta_s / dt$

Since the stator flux is along the *x*-axis which results in $\phi_y = 0$ and $\phi_x = \phi_s$. The presented control strategy is based on simplified stator voltage equations described in stator flux oriented *x-y* coordinates:

$$\begin{cases} v_x = R_s i_x + \dfrac{d\phi_s}{dt} \\ v_y = R_s i_y + \Omega_s \phi_s \end{cases} \tag{30}$$

The electromagnetic torque can be expressed by the following formula:

$$T_{em} = p\phi_s i_y \tag{31}$$

The above equations show that the v_x component has influence only on the change of stator flux magnitude ϕ_s , and the component v_y if the term $\Omega_s \phi_s$ is decoupled can be used for torque adjustment.

Considering the above simple model of DSSM, the Fig. 5 shows the stator flux and electromagnetic torque control loops for the DTC-SVM in *x-y* reference.

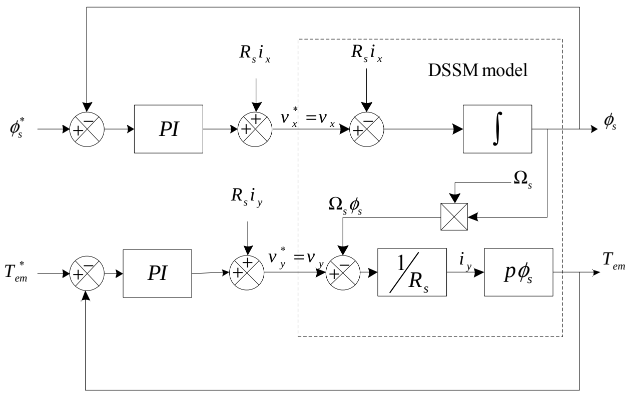

Fig.5 flux and torque control loop with two *PI* controllers in *x-y* reference frame.

V. SPEED ESTIMATION BASED ON LUENBERGER OBSERVER

The Luenberger observer will be used to estimate the rotor position and rotor speed of DSSM. The Luenberger observer is based on the error of the actual position and actual speed and their estimated values which must be converged toward zero. Fig. 6 shows a schematic diagram of mechanical state variables estimation using Luenberger observer.

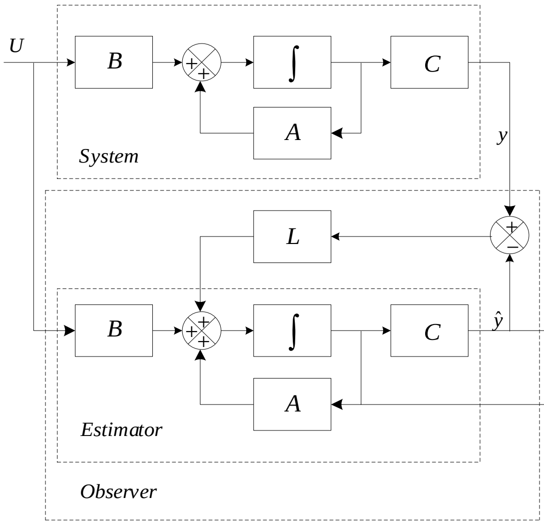

Fig. 6. Luenberger structure for angular position and speed estimation.

The state equations of simplified model of DSSM are written as:

$$\begin{cases} \dot{x} = Ax + BU \\ y = Cx \end{cases} \quad (32)$$

With:

$$x = \begin{bmatrix} \theta & \Omega & T_L \end{bmatrix}^T, \; U = i_q, \; B = \begin{bmatrix} 0 & pM_{fd} i_f / J & 0 \end{bmatrix}^T$$

$$A = \begin{bmatrix} 0 & p & 0 \\ 0 & -f/J & -1/J \\ 0 & 0 & 0 \end{bmatrix}, \; C = \begin{bmatrix} 1 & 0 & 0 \\ 0 & 1 & 0 \\ 0 & 0 & 0 \end{bmatrix}$$

The Luenberger observer is given by the following system:

$$\begin{cases} \dot{\hat{x}} = A\hat{x} + Bu + L(y - \hat{y}) \\ \hat{y} = C\hat{x} \end{cases} \quad (33)$$

With:

$$L = \begin{bmatrix} 0 & 0 & 0 \\ l_1 & l_2 & 0 \\ l_3 & 0 & 0 \end{bmatrix}$$

with : l_1, l_2, l_3 are the observer gains.

And: l_1, l_2, l_3 are the observer gains.

This observer can be established from the DSSM model as follows:

$$\begin{cases} \dfrac{d\hat{\theta}}{dt} = p\hat{\Omega} \\ \dfrac{d\hat{\Omega}}{dt} = \dfrac{1}{J}(T_{em} - \hat{T}_L) - \dfrac{f}{J}\hat{\Omega} + l_1(\Omega - \hat{\Omega}) + l_2(\theta - \hat{\theta}) \\ \dfrac{d\hat{T}_L}{dt} = l_3(\theta - \hat{\theta}) \end{cases} \quad (34)$$

The Fig. 7 represents the total configuration of the five-level DTC-SVM of sensorless DSSM.

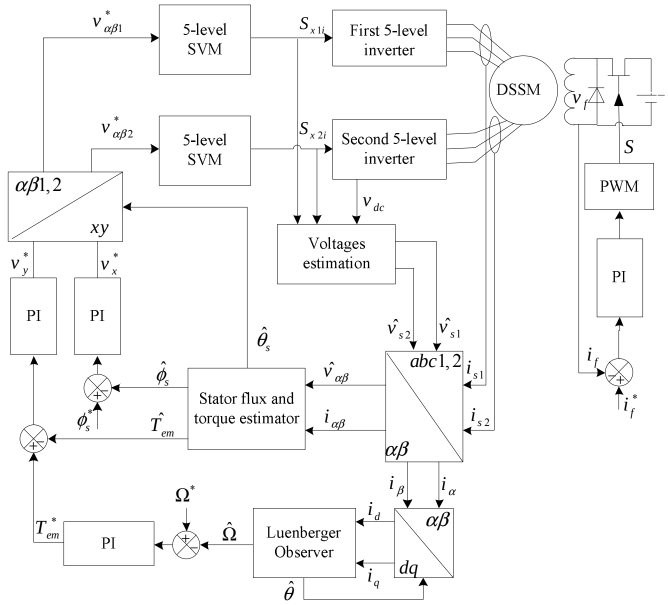

Fig. 7. Five-level DTC-SVM scheme for sensorless DSSM.

VI. Comparative study between two-level DTC and two-level DTC-SVM

The aim of this section is to compare the two-level DTC for sensorless DSSM with the two-level DTC-SVM for sensorless DSSM. The DC side of the inverter is supplied by a constant DC source $v_{dc}=600V$. The observer gains [l_1 l_2 l_3] are chosen as follows: [100000 100 1] to satisfy convergence conditions. Two situations are considered:

Situation 1: Step change in load torque. The DSSM is accelerating from standstill to reference speed *100*rad/s. The system is started with full load torque (T_L = *11*N.m). Afterwards, a step variation on the load torque (T_L = *0*N.m) is applied at time *t*=*1*s.

The multiphase drive performances are presented in Figs. 8 and 9 for the two-level DTC and the two-level DTC-SVM respectively. The decoupling control is clearly maintained during load torque variation. The speed response is merged with the reference one and the flux is very similar to the nominal value. It can be observed also that the estimated speed can track the actual speed accurately with minor error. However, the DTC-SVM for DSSM decreases considerably the torque ripple in comparison with basic DTC.

Situation 2: Step change in reference speed. To test the speed evolution of the system, the DSSM is accelerate from standstill to reference speed (*100*rad/s) afterwards it is decelerate to the inverse rated speed (-*100*rad/s) at t=*1.5*s.

The performances for the DTC are presented in Fig. 8, for the DTC-SVM see Fig. 9. The control scheme ensures good quality results during reference speed inversion period. The speed response is smooth without fluctuations and the flux is insensitive to torque transients and is without significant ripple. The estimated speed follows the actual speed. It found once more, that the DTC-SVM reduces significantly the flux and torque ripples in comparison to the conventional DTC.

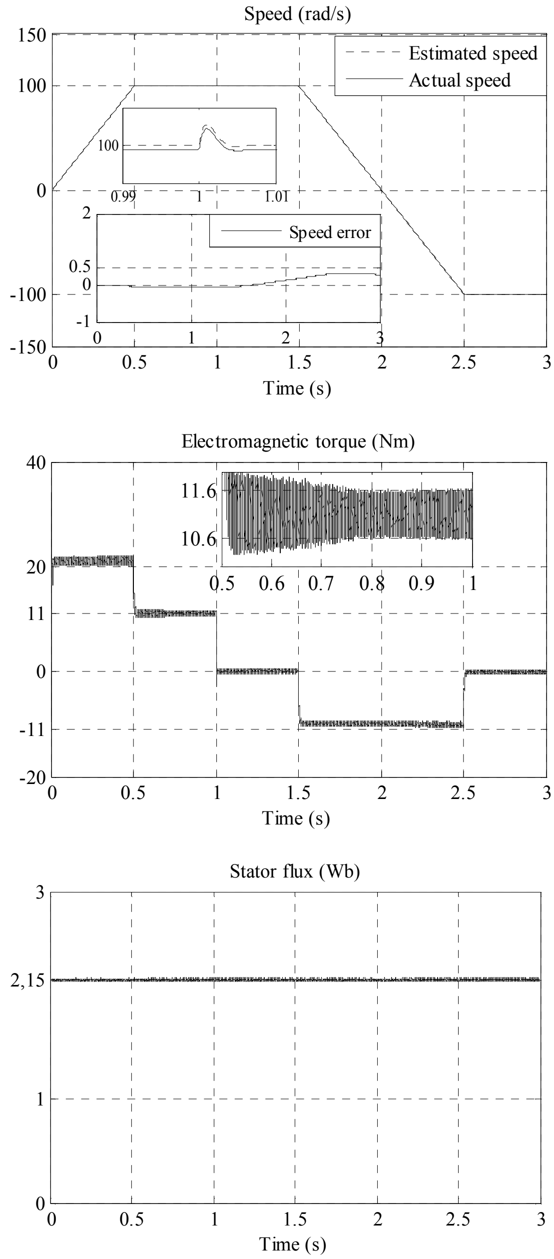

Fig. 8 dynamic responses of two-level conventional DTC for sensorless DSSM.

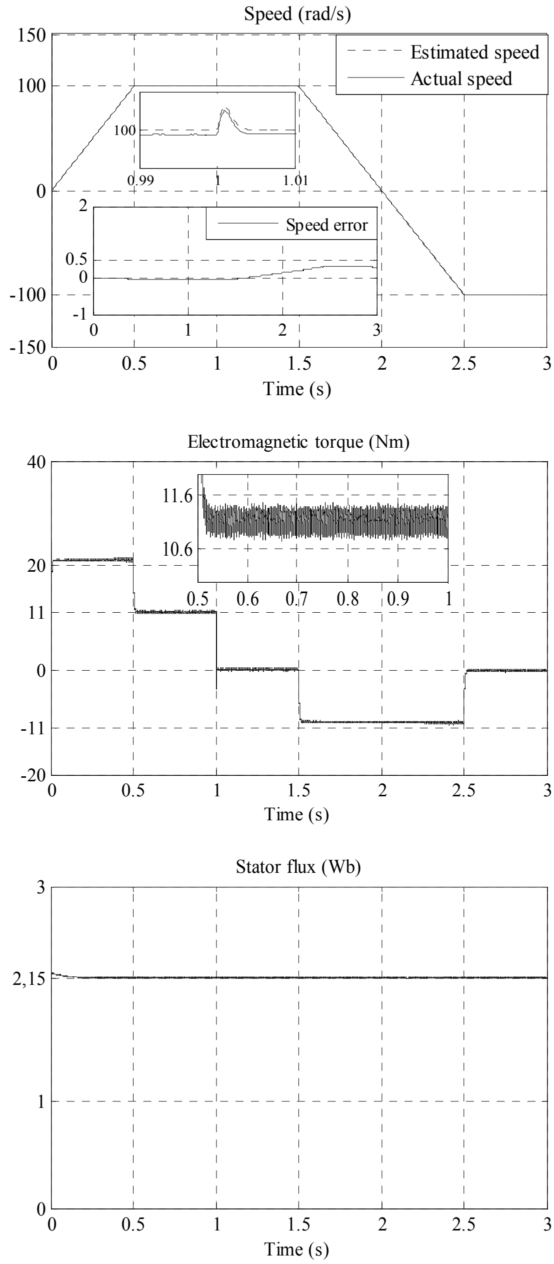

Fig. 9 dynamic responses of two-level DTC-SVM for sensorless DSSM.

VII. COMPARATIVE STUDY BETWEEN TWO-LEVEL DTC-SVM AND FIVE-LEVEL DTC-SVM

In this section the two-level DTC-SVM for sensorless DSSM is compared with the five-level DTC-SVM. The inverter is supplied by a constant DC source. In multilevel case, this source is equally shared between DC side capacitors such as each capacitor voltage takes *150V*. In order to simulate these control methods the same two situations, defined above, are applied during DSSM operating.

The obtained results are presented in Fig. 9 for the two-level DTC-SVM and Fig. 10 for the five-level DTC-SVM. The above results show that the actual speed response is in good agreement with reference speed. The decoupling is ensured in the beginning and during all the control process.

The error between the rotor speed estimated by the Luenberger observer and its real value is kept small around zero. The comparison between Fig. 9 and Fig. 10 reveals that the flux and torque ripples of the proposed five-level DTC-SVM are less than those obtained with a two-level inverter.

The five-level DTC-SVM without speed sensor method decreases considerably the torque ripple and ensures good decoupling between flux linkage and electromagnetic torque. However, the five-level DCI has an inherent unbalancing problem among its DC capacitor voltages. This problem results in collapse of some voltages and the rise of others due to the non-uniform power drawn from capacitors. For this reason the five-level DTC-SVM without speed sensor based on balancing strategy is proposed to solve this drawback.

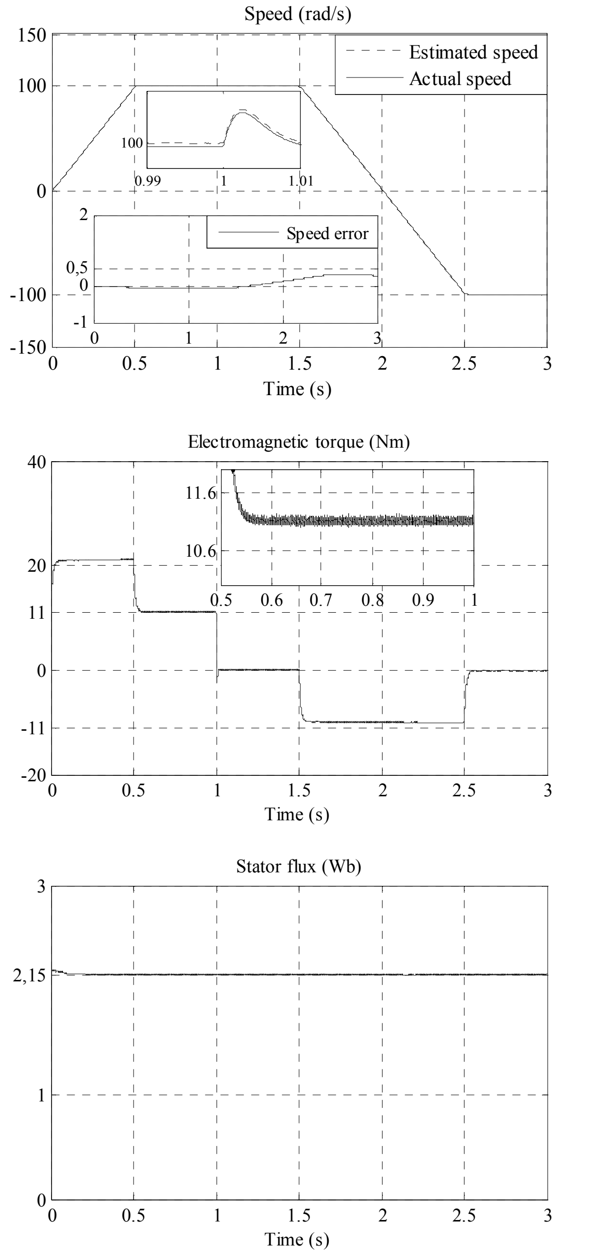

Fig. 10 dynamic responses of five-level DTC-SVM for sensorless DSSM.

VIII. Voltage Balancing Theory

The proposed SVM-based DC-capacitor voltage balancing strategy is founded on the minimization of a cost function J using an appropriate selection of redundant switching states of the five-level DCI over a switching period [6].

The total energy of the four condensers is given by:

$$E = \frac{1}{2}\sum_{j=1}^{4} C_j v_{cj}^2 \tag{35}$$

Assuming that all capacitors are identical, $C_1=C_2=C_3=C_4=C$, the energy E is minimal if all the capacitor voltages are balanced. Indeed:

$$E_{\min} = \frac{1}{2} C \frac{v_{dc}^2}{4} \tag{36}$$

The property of minimization of energy can be employed for the balancing of the capacitor voltages. For this reason, a cost function J_k is defined. This function is based on the quadratic sum of the differences between the capacitor voltages and their reference values $(v_{dc}/4)$ [6]. So, J_k is expressed by:

$$J = \frac{1}{2} C \sum_{j=1}^{4}\left(v_{cj} - \frac{v_{dc}}{4}\right)^2 \tag{37}$$

Based on a suitable choice of the redundant vectors, the function J_k can be minimized to zero and the capacitor voltages will be maintained at their reference values. The mathematical condition ensuring the convergence of the cost function J_k at its minimal value is given by:

$$\frac{dJ_k}{dt} = C \sum_{j=1}^{4} \Delta v_{cj} \frac{dv_{cj}}{dt} \le 0 \tag{38}$$

Where: $\Delta v_{cj} = v_{cj} - v_{dc}/4$

The current in each condenser is defined by:

$$i_{cj} = C\frac{dv_{cj}}{dt} \tag{39}$$

Using (39), the equation (38) becomes:

$$\sum_{j=1}^{4} \Delta v_{cj} i_{cj} \le 0 \tag{40}$$

Where: i_{cj} is the current through capacitor C_j.

The capacitor currents i_{cj} in (40) are affected by the DC-side intermediate branch currents i_{k3}, i_{k2} and i_{k1}. These currents can be calculated if the switching states used in the switching pattern are known. Thus, it is advantageous to express (40) in terms of i_{k3}, i_{k2} and i_{k1}. The DC-capacitor currents are expressed as:

$$\begin{cases} i_{c4} = i_{c3} + \sum_{k=1}^{2} i_{k3} \\ i_{c3} = i_{c2} + \sum_{k=1}^{2} i_{k2} \\ i_{c2} = i_{c1} + \sum_{k=1}^{2} i_{k1} \end{cases} \tag{41}$$

Considering a constant DC bus voltage, it yields:

$$C\sum_{j=1}^{4}\frac{dv_{cj}}{dt} = \sum_{j=1}^{4} i_{cj} = 0 \tag{42}$$

The capacitor currents are given by:

$$i_{cj}=\frac{1}{4}\sum_{m=1}^{3} m\left(\sum_{k=1}^{2} i_{km}^{S_k^i}\right)-\sum_{m=j}^{3}\left(\sum_{k=1}^{2} i_{km}^{S_k^i}\right) \tag{43}$$

Where: $m=1, 2, 3$. Let us replace i_{cj} given by (43) in (40), the balancing condition of the capacitor voltages becomes:

$$\sum_{j=1}^{4}\Delta v_{cj}\left(\frac{1}{4}\sum_{m=1}^{3} m\left(\sum_{k=1}^{2} i_{km}^{S_k^i}\right)-\sum_{m=j}^{3}\left(\sum_{k=1}^{2} i_{km}^{S_k^i}\right)\right)\leq 0 \tag{44}$$

It is known also:

$$\sum_{j=1}^{4}\Delta v_{cj}=0 \tag{45}$$

By replacing Δv_{c4} extracted from (45) in (44), the condition of balancing can be reduced to:

$$\sum_{j=1}^{3}\Delta v_{cj}\left(\sum_{m=j}^{3}\left(\sum_{k=1}^{2} i_{km}^{S_k^i}\right)\right)\geq 0 \tag{46}$$

The application of the average operator on the equation (46) during one commutation period T gives:

$$\frac{1}{T}\sum_{KT}^{(K+1)T}\Delta v_{cj}\left(\sum_{m=j}^{3}\left(\sum_{k=1}^{2} i_{km}^{S_k^i}\right)\right)dt\geq 0 \tag{47}$$

If it is admitted that the period of commutation is weak in front of the response time of the capacitor voltages, the capacitor voltages can be regarded as constants [6], and consequently the equation (47) will be simplified to:

$$\sum_{j=1}^{3}\Delta v_{cj}(K)\left(\sum_{m=j}^{3}\frac{1}{T}\int_{KT}^{(K+1)T}\left(\sum_{k=1}^{2} i_{km}^{S_k^i}\right)dt\right)\geq 0 \tag{48}$$

Or

$$\sum_{j=1}^{3}\Delta v_{cj}(K)\left(\sum_{m=j}^{3}\left(\sum_{k=1}^{2}\bar{i}_{km}^{S_k^i}(K)\right)dt\right)\geq 0 \tag{49}$$

Where:
$\Delta v_{cj}(K)$: is the voltage drift of C_j at sampling period K. $\bar{i}_{km}^{S_k^i}(K)$: is the averaged value of the j^{th} DC-side intermediate branch current.

The currents $\bar{i}_{km}^{S_k^i}(K)$ should be computed for different combinations of adjacent redundant switching states over a sampling period and the best combination which maximizes (49) is selected.

If the reference vector is in the triangle $\Delta_q^{S_k^i}$, $q\in\{1,...,16\}$, and $t_{x_k}^{\Delta_q^{S_k^i}}, t_{y_k}^{\Delta_q^{S_k^i}}, t_{z_k}^{\Delta_q^{S_k^i}}$ are the application times of the vectors $u_{x_k}^{\Delta_q^{S_k^i}}, u_{y_k}^{\Delta_q^{S_k^i}}, u_{z_k}^{\Delta_q^{S_k^i}}$ respectively, $\bar{i}_{k3}^{S_k^i}, \bar{i}_{k2}^{S_k^i}$, and $\bar{i}_{k1}^{S_k^i}$ currents are expressed by:

$$\begin{bmatrix}\bar{i}_{k3}^{S_k^i}\\ \bar{i}_{k2}^{S_k^i}\\ \bar{i}_{k1}^{S_k^i}\end{bmatrix}=\frac{1}{T}\begin{bmatrix} i_{k3x}^{S_k^i} & i_{k3y}^{S_k^i} & i_{k3z}^{S_k^i}\\ i_{k2x}^{S_k^i} & i_{k2y}^{S_k^i} & i_{k2z}^{S_k^i}\\ i_{k1x}^{S_k^i} & i_{k1y}^{S_k^i} & i_{k1z}^{S_k^i}\end{bmatrix}\begin{bmatrix} t_{kx}^{\Delta_q^{S_k^i}}\\ t_{ky}^{\Delta_q^{S_k^i}}\\ t_{kz}^{\Delta_q^{S_k^i}}\end{bmatrix} \tag{50}$$

Where $i_{kmx}^{S_k^i}, i_{kmy}^{S_k^i}$ and $i_{kmz}^{S_k^i}$ are the charging currents to the states of commutation x_k, y_k and z_k in the triangle $\Delta_q^{S_k^i}$ minimizing the function cost J_k.

For the conventional five-level DTC-SVM the cost function is given by:

$$J_k=\sum_{j=1}^{3}\Delta v_{cj}(K)\left(\sum_{m=j}^{3}\left(\sum_{k=1}^{2}\bar{i}_{km}^{S_k^i}(K)\right)\right)dt \tag{51}$$

This section aims to demonstrate the effectiveness of the proposed DTC-SVM strategy to control and prevent drift of DC capacitor voltages. Fig. 11 shows a schematic block of the five-level DTC-SVM balancing system including the DC capacitor voltage control block.

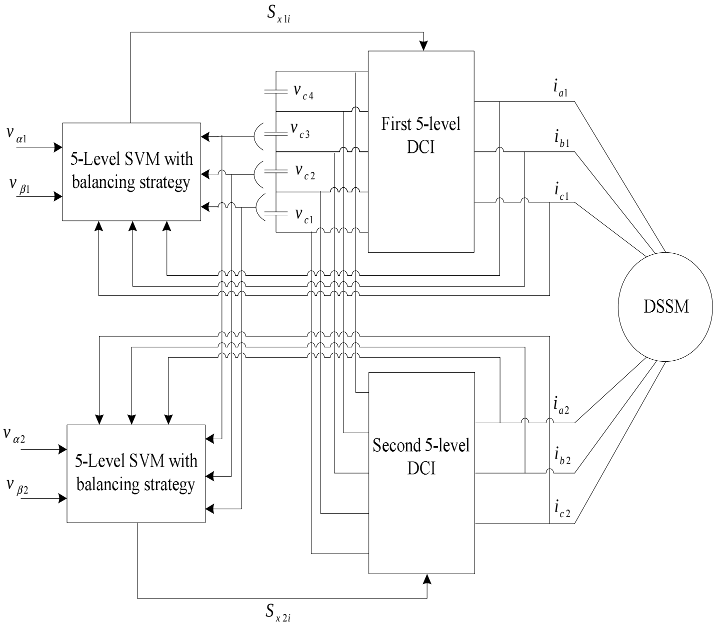

Fig. 11 schematic representation of the five-level DTC-SVM with balancing strategy of DSSM.

IX. Simulation Results

Simulations were performed to show the behavior of the double star synchronous machine fed by two five levels DCI controlled via space vector modulation. The proposed direct torque control is based on speed estimation using Luenberger observer.

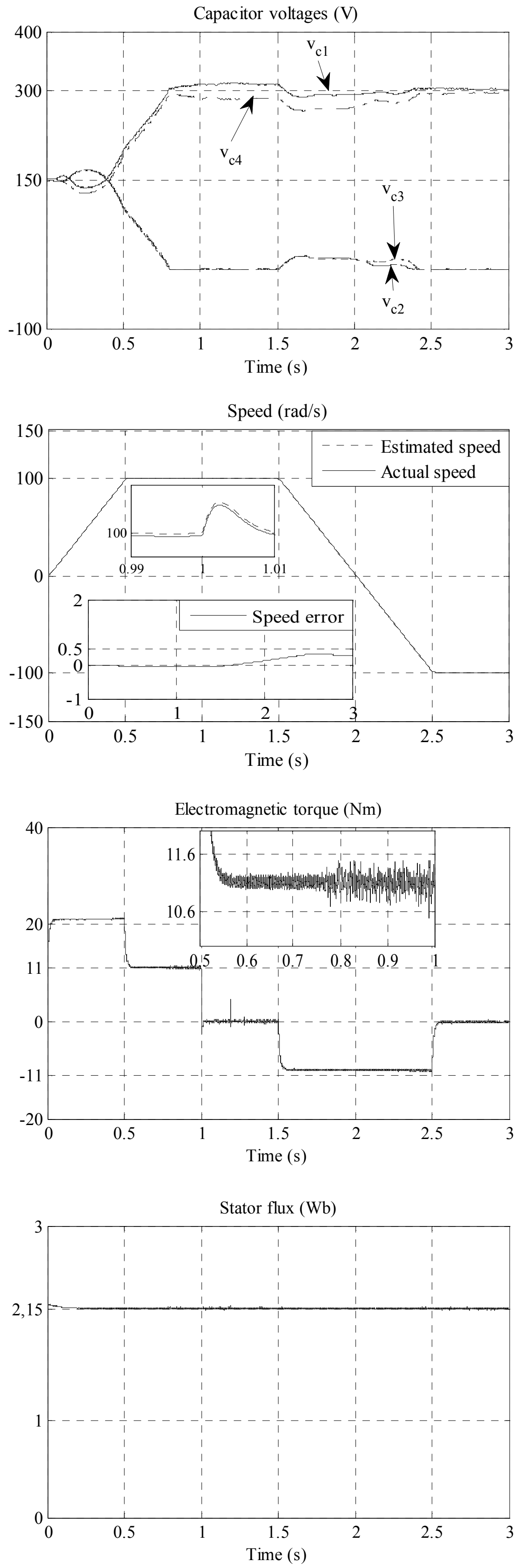

Fig. 12 dynamic responses of five-level DTC-SVM without balancing strategy for sensorless DSSM.

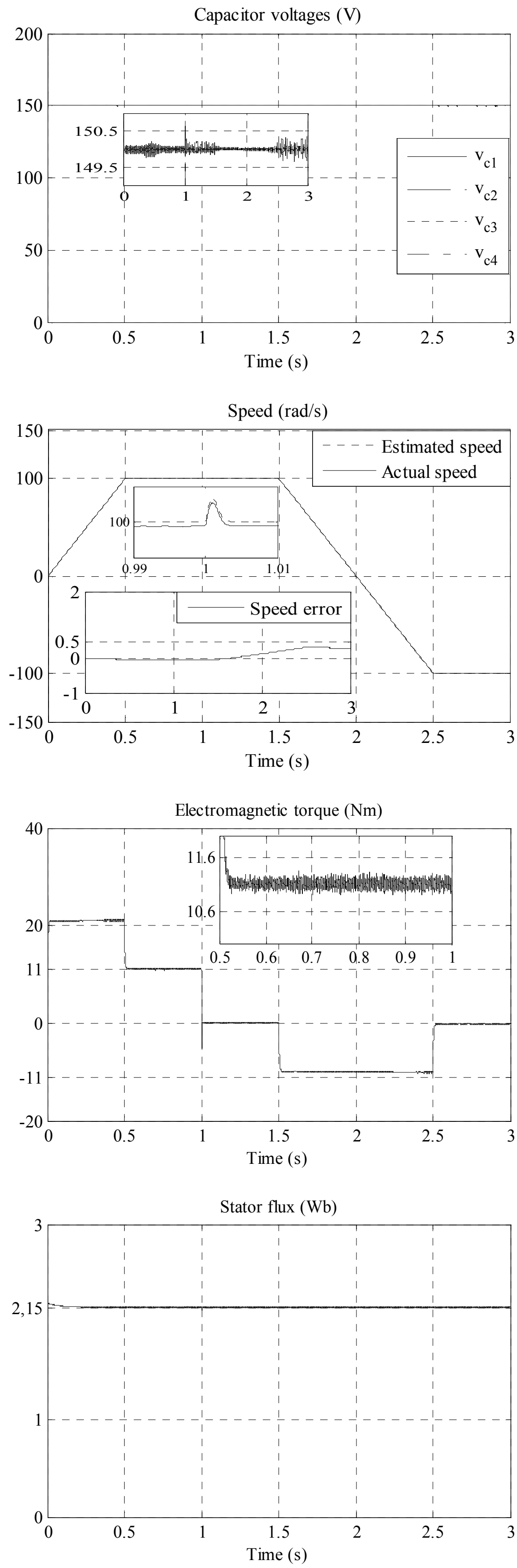

Fig. 13 dynamic responses of five-level DTC-SVM with balancing strategy for sensorless DSSM.

A. Dynamic performances during speed and load torque variation:

The DSSM is accelerating from standstill to reference speed *100*rad/s. At first, *11 Nm* load is applied to the motor. At *t=1*s, the load is completely removed from the motor shaft. Afterwards it is decelerate to the inverse rated speed (-*100*rad/s) at time *t=1.5*s. The multiphase drive performances are presented in Fig. 12 for the five-level DTC-SVM without balancing strategy and Fig. 13 for the five-level DTC-SVM with balancing strategy.

One can notice that the proposed method performances are very satisfactory. The rejection of disturbance is very efficient. It is clear from the figures that the motor is regulated to the desired speed and the flux is maintained constant independently from the torque variations. Thus decoupling between stator flux linkage and torque is guaranteed for the nominal load.

The problem of the unbalance capacitor voltages and its consequence on electromagnetic torque harmonics appears in Fig. 12. This problem it is solve in Fig. 13. It is clear that each capacitor voltage follows closely to its reference voltage value. Consequently, the torque ripple decreases considerably using the proposed balancing strategy.

It can be seen that, the rotor speed error converge to zero rapidly. Good speed estimation is achieved at the high speed region with rated load. Remarkably, the designed sensorless control scheme is robust against load torque application.

B. Dynamic performances during low speed operation:

In order to verify the robustness of the proposed control using Luenberger observer, a low speed test has been performed. The DSSM is accelerating from standstill to reference speed *10*rad/s. The system is started with full load torque (T_L= *11*N.m), a step variation on the load torque (T_L= *0*N.m) is applied at time *t=1*s. Afterwards, the DSSM is accelerated again to reference speed *100*rad/s at time *0.3*s. Finally, it is decelerate to the reference speed (*-10* rad/s) at time *t=1.2*s.

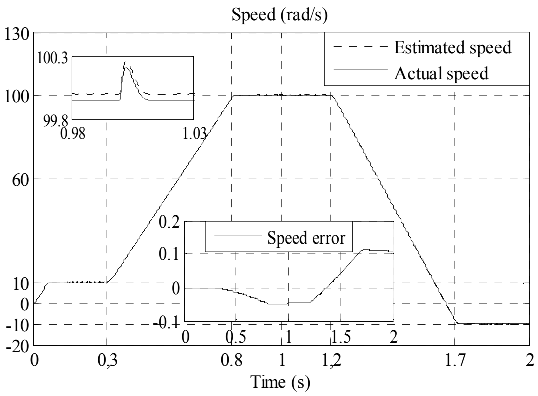

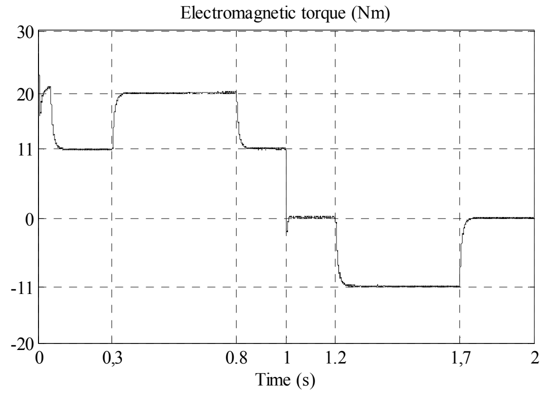

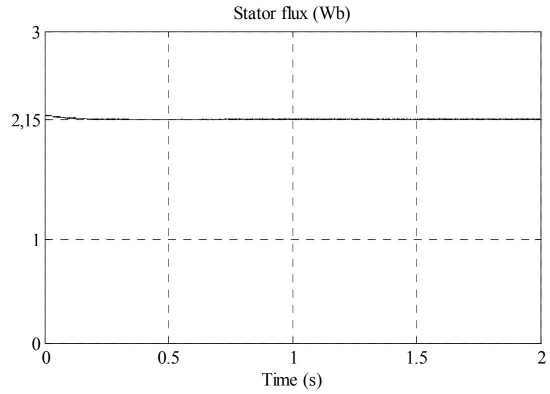

Fig. 14 dynamic responses of five-level DTC-SVM for sensorless DSSM for low speed.

The performances of the five-level DTC-SVM for sensorless DSSM for low speed using Luenberger observer are presented in Fig. 14. Simulation results show that the sensorless controller is indeed effective to drive the multiphase machine to track the speed reference even in low speed. The operation at low speed does not influence the estimation of the rotor speed. The estimated speed reaches the real one with very small steady-state error and good dynamics. Furthermore, the proposed observer is of high accuracy and robustness against load torque variation.

X. Conclusion

In this paper, a multilevel direct torque of sensorless salient-pole DSSM, fed by two five-level diode-clamped inverters has been investigated. The multilevel diode-clamped inverter has an inherent problem of DC-link capacitors voltages fluctuations. This problem can be solved in satisfactory way by using a simplified multilevel DTC-SVM algorithm equipped by a balancing strategy. This solution has offered the opportunity to equalize the different input DC voltages of the inverter and improve the performances of the multiphase machine. The simulation results conclude that the proposed DTC is able to carry out the voltage-balancing task with no requirement for additional auxiliary power circuitry. Furthermore, the proposed control scheme decreases considerably the torque ripples and assures good speed tracking without overshoot. The decoupling between the stator flux and the electromagnetic torque is maintained, confirms the good performances of the developed drive systems. In addition, the simulation results have shown that the proposed sensorless multiphase drive has a satisfactory dynamic response over a wide speed range.

Appendix 1. List of principal symbols

v_{1a}, v_{1b}, v_{1c}	: Stator voltages of the first winding.
v_{2a}, v_{2b}, v_{2c}	: Stator voltages of the second winding.
v_{α}, v_{β}	: The α-β components of stator voltage.
v_d, v_q	: The *d*-*q* components of stator voltage.
v_x, v_y	: The *x*-*y* components of stator voltage.
i_{1a}, i_{1b}, i_{1c}	: Stator currents of the first winding.
i_{2a}, i_{2b}, i_{2c}	: Stator currents of the second winding.
i_{α}, i_{β}	: The α-β components of stator current.
i_d, i_q	: The *d*-*q* components of stator current.
i_x, i_y	: The *x*-*y* components of stator current.
ϕ_{1a}, ϕ_{1b}, ϕ_{1c}	: Stator flux of the first winding.
ϕ_{2a}, ϕ_{2b}, ϕ_{2c}	: Stator flux of the second winding.
$\phi_{\alpha}, \phi_{\beta}$	: The α-β components of stator flux.
ϕ_d, ϕ_q	: The *d*-*q* components of stator flux.
ϕ_x, ϕ_y	: The *x*-*y* components of stator flux.
v_f, i_f	: Voltage and current of rotor excitation.
ϕ_f	: Flux of rotor excitation.
T_{em}, T_L	: Electromagnetic and load torques.
Ω	: Rotor speed.
ω	: Rotating speed of rotor flux linkage.
ω_s	: Rotating speed of stator flux linkage.
θ_s	: Angular position.
δ	: Angle between rotor and stator flux.
$\gamma = \pi/6$	: Angle between first and second stators.
R_s	: Stator resistance.
R_f	: Rotor resistance.
L_d, L_q	: *d*-*q* stator inductances.
L_f	: *d*-axis rotor inductance.
p	: Pole pair number.
J	: Moment inertia.
f_r	: Friction coefficient.
M_{fd}	: Mutual inductance between *d*-axis for each stator and rotor.

Appendix 2. DSSM parameters

p_n=5kW, v_n=232V, p=1, R_s=2.35 Ω, R_f=30.3Ω, L_d=0.3811H, L_q=0.211H, L_f=15H, M_{fd}=2.146H, J=0.05Nms^2/rad, f_r=0.001Nms/rad, $i_f^* = 1A$.

REFERENCES

[1] G. Rigatos, P. Siano, P. Wira, "Nonlinear H-infinity control of multi-phase electric machines," International Federation of Automatic Control, vol. 49, n. 27, pp. 109-115, 2016..
[2] E. Benyoussef, A. Meroufel, S. Barkat, "Neural network and fuzzy logic direct torque control of sensorless double star synchronous machine," Revue Roumaine des Sciences Techniques Serie Electrotechnique et Energetique, vol. 61, no. 3, pp. 239-243, 2016.
[3] R. Manuel, B. Federico, J. Mario, G. Manuel, M. Cristina, "Trade-offs analysis in predictive current control of multi-phase induction machines," Control Engineering Practice, vol. 81, pp. 105-113, 2018.
[4] A. Abdel-Khalik, S. Gadoue, "Improved flux pattern by third harmonic injection for multiphase induction machines using neural network," Alexandria Engineering Journal, vol. 50, pp. 163-169, 2011.
[5] O. Sekhar, and K. Chandra, "A novel five-level inverter topology for DTC induction motor drive," IEEE International Conference on Advanced Communication Control and Computing Technologies, pp. 392-396, 2012.
[6] E. Benyoussef, S. Barkat, "Direct torque control based on space vector modulation with balancing strategy of dual star induction motor," Revue Roumaine des Sciences Techniques Serie Electrotechnique et Energetique, vol. 67, n. 1, pp. 15-20, 2022.
[7] S. Deepak, A. Bhat, A. Aijaz, L. Nitin, "Capacitor voltage balancing in neutral-point clamped rectifier using modified modulation index technique," Energy Conversion and Management, vol. 79, pp. 721-730, 2014.
[8] C. Xianqing, F. Liping, "New DTC scheme based on SVM with sliding-mode observer for induction motors," Proceedings of the IEEE International Conference on Automation and Logistics Shenyang, China, pp. 1484-1488, 2009.
[9] B. Qu, L. Hong, "Design of sensorless permanent magnet synchronous motor control system," Electronics and Signal Processing, LNEE, vol. 97, pp. 533-539, 2011.
[10] J. Holtz, J. Quan, "Drift and parameter compensation flux estimator for persistent zero stator frequency operation of sensorless controlled induction motors," IEEE Transactions on Industrial Application, vol. 39, no. 4, pp. 1052-1060, 2003.
[11] X. Zhuang, M. Rahman, "Comparison of a sliding observer and a Kalman filter for direct-torque-controlled IPM synchronous motor drives," IEEE, Transactions on Industrial Electronics, vol. 59, no. 11, pp. 4179-4188, 2012.
[12] Subodh K., Kiran K., "Five-Phase Induction Motor DTC-SVM scheme with PI Controller and ANN controller," Procedia Technology, vol. 25, pp. 816-823, 2016.

Contribution of individual authors

Elakhdar BENYOUSSEF : In 2015 he joined the Department of Electrical Engineering, University Kasdi Merbah of Ouargla (Algeria). His research interests are in modeling and robust control of dual three phase synchronous and induction motors and converters.

Said BARKAT : He is currently Professor of electrical engineering in university of M'sila (Algeria). His current research interests are in the field of power electronics, renewable energies, multiphase drives, and advanced control theory and applications.